Improved resolution in Bayesian lithology/fluid inversion from prestack seismic data and well observations:

Part I - Methodology

Marit Ulvmoen* and Henning Omre*

*Norwegian University of Science and Technology,

N-7491 Trondheim,

Norway.

E-mail: ulvmoen@math.ntnu.no; omre@math.ntnu.no

ABSTRACT

Focus is on lithology/fluid inversion with spatial coupling from prestack seismic AVO data and well observations. The inversion is defined in a Bayesian setting where the complete solution is the posterior model. The prior model for the lithology/fluid characteristics is defined as a profile Markov random field model with lateral continuity. Each vertical profile is further given as a nonhomogeneous Markov chain model upward through the reservoir. The likelihood model is defined profilewise, and it relates the lithology/fluid characteristics to the seismic data via a set of elastic material parameters. The likelihood model is approximated. The resulting approximate posterior model is explored using an efficient block Gibbs simulation algorithm. The inversion approach is evaluated on a synthetic realistic 2D reservoir. Seismic

data and well observations are integrated in a consistent way in the inversion. The resolution in the inversion results is considerably improved, and lithology/fluid units of thickness 1-3 ms can be identified. The simulation algorithm is partially analytically tractable; hence full 3D studies will be feasible.

INTRODUCTION

Prediction of lithology/fluid (LF) characteristics in a petroleum reservoir with associated uncertainty is important for development of reserves. LF characteristics are normally predicted based on geological understanding of the reservoir combined with well observations and seismic data. The classification problem is ill-posed as several LF configurations may produce the same seismic data. The objective of the study is to infer LF classes in a target zone given well observations and seismic AVO data. The inversion is defined in a Bayesian setting where prior knowledge about the LF characteristics is combined with information contained in the observed data.

Bayesian frameworks are commonly used for inversion of LF characteristics from prestack seismic data. In Eidsvik et al. (2004) the inversion is defined in a horizontal 2D setting where the prior is a Markov random field. In this horizontal 2D model, vertical couplings due to convolution of the seismic data are ignored. In Larsen et al. (2006) the inversion is defined in a 1D vertical setting where the vertical dependencies within the LF classes are modeled as a Markov chain prior model. The inversion is solved approximately including vertical deconvolution of the seismic data. In Buland et al. (2008) the inversion is solved in a 3D setting using a vertically coupled likelihood model and a locationwise prior model which entails that no prior spatial information about the LF classes is taken into account. In González et al. (2008) an algorithmic approach to lithology inversion from stacked seismic data is defined. The approach is based on a multi-point spatial prior model for lithology and sequential trial-and-error conditioning to the seismic data. The conditioning procedure may be very computer demanding and is expected to be infeasible for high dimensional AVO seismic data needed for classification of fluid filling. Moreover, the efficiency of the conditioning is

unclear due to lack of formality in the definition of the algorithm. A thorough introduction to LF inversion from seismic data is given in Avseth et al. (2005).

In the current study the inversion is solved using a spatially coupled prior model for the LF classes. This model formulation appears to be more in accordance with the geologists understanding of the reservoir geometry, and moreover, it entails that well observations are given influence beyond the well locations. One particular focus is on identification of thin, laterally extensive features of the reservoir, which in our study is defined to be shale units. A spatially coupled prior model for the LF classes will make improved resolution in the inversion possible.

The target zone is discretized into vertical profiles and lateral horizons. Vertical couplings of the LF classes are modeled by a Markov chain prior model. Lateral continuity of the LF classes in the horizons is further modeled by a profile Markov random field prior model. The assumptions above entail that the 3D LF model falls within the class of Markov random fields, see Besag (1974).

The likelihood model is approximated such that the upward-downward algorithm used to assess the posterior model in Larsen et al. (2006) can be used to explore the vertical profiles. Laterally, a block Gibbs simulation algorithm is used. Realizations and prediction of the most probable combination of LF classes with associated uncertainties can be assessed by simulation based inference. The study draws heavily on previous work on AVO inversion in Buland and Omre (2003) and Larsen et al. (2006).

The major contribution of the current study is on expanding the model in Larsen et al. (2006) into 3D, where lateral continuity of the LF classes is modeled. It is demonstrated that by modeling lateral continuity, considerable better resolution in the LF class prediction can be

4

obtained. The inversion approach is evaluated empirically on synthetic seismic data. The inversion approach is further evaluated on real seismic data from a reservoir offshore Norway in Ulvmoen et al. (2009).

NOTATION

Denote the target zone in 3D by $\mathcal{D}$, and let it be discretized by the lattice $\mathcal{L}_\mathcal{D}$ divided into vertical profiles and lateral horizons. The profiles are discretized downward by the regular lattice $\mathcal{L}_\mathcal{D}^t : \{1, \ldots, T\}$, where the reflection time t corresponds to the seismic sampling. The lateral horizons are further discretized by the regular lattice $\mathcal{L}_\mathcal{D}^\mathbf{x}$, with $\mathcal{L}_\mathcal{D}^\mathbf{x}$ corresponding to the seismic survey positions.

The LF characteristic in lattice node $(\mathbf{x}, t) \in \mathcal{L}_\mathcal{D}$ is denoted $\pi_{\mathbf{x},t}$, discretized into a set of LF classes $\pi_{\mathbf{x},t} \in \{\pi^1, \ldots, \pi^L\}$. The complete set of LF classes in the 3D target zone is further represented by $\boldsymbol{\pi} : \{\pi_{\mathbf{x},t}; (\mathbf{x}, t) \in \mathcal{L}_\mathcal{D}\}$.

We assume well observations to be available along vertical well profiles at n well locations represented by $\mathcal{K} \subset \mathcal{L}_\mathcal{D}^\mathbf{x}$, which coincide with some of the lattice locations in $\mathcal{L}_\mathcal{D}^\mathbf{x}$. The well data are denoted by $\mathbf{d}^w$, and they contain LF observations at $t \in \mathcal{L}_\mathcal{D}^t$ along the well profiles.

The seismic data are assumed to be true amplitude processed such that the prestack amplitudes represent band-limited primary reflection strengths. The data are also assumed to be prestack migrated and transformed from offsets to reflection angles. The seismic prestack gather is represented by $\mathbf{d}^s$ containing the seismic samples in $\mathcal{L}_\mathcal{D}$ for a set of m reflection angles $\boldsymbol{\theta} : \{\theta_1^\circ, \ldots, \theta_m^\circ\}$. The joint well observations and seismic data are denoted by $\mathbf{d} : \{\mathbf{d}^w, \mathbf{d}^s\}$.

An isotropic, elastic medium is completely described by three elastic parameters, for example

P-wave velocity, S-wave velocity, and density. In order to link the LF classes and the seismic data, elastic properties are defined at each location in $\mathcal{L}_{\mathcal{D}}$. Let $\boldsymbol{m}_{\mathbf{x},t}$ represent the log transform of the three elastic parameters in lattice node $(\mathbf{x},t) \in \mathcal{L}_{\mathcal{D}}$. The complete set of elastic parameters is represented by $\mathbf{m} : \{\mathbf{m}_{\mathbf{x},t}; (\mathbf{x},t) \in \mathcal{L}_{\mathcal{D}}\}$.

The term $p(\cdot)$ is used as a generic term for probability. In particular, $p(\pi_{\mathbf{x},t})$ denotes the probability for the various LF classes $\pi_{\mathbf{x},t} \in \{\pi^1, \ldots, \pi^L\}$, and correspondingly, $p(\boldsymbol{\pi})$ is a multivariate probability for $\boldsymbol{\pi}$, the complete set of LF classes. For discrete variables $p(\cdot)$ will be the probability mass function (pmf), while it will be the probability density function (pdf) for continuous variables.

STOCHASTIC MODEL

The objective of the study is to predict the LF characteristics in a target zone from well observations and seismic prestack data. We do this in a Bayesian setting, combining available prior knowledge about $\boldsymbol{\pi}$ with the information contained in the data $\mathbf{d}$. In this setting, the complete solution is the posterior model which is expressed

$$p(\boldsymbol{\pi}|\mathbf{d}) = \text{const} \times p(\mathbf{d}|\boldsymbol{\pi})\, p(\boldsymbol{\pi}) \tag{1}$$

where $p(\mathbf{d}|\boldsymbol{\pi})$ is the likelihood model and $p(\boldsymbol{\pi})$ is the prior model. The constant is a normalizing constant which is usually difficult to determine; hence the posterior model is normally explored through stochastic simulation where direct calculation of the constant is avoided. From the posterior model, the probability of any combination of LF classes in the target zone can be calculated, and in particular, the most probable combination can be identified.

6

It is also possible to generate a set of realizations of the LF characteristics representing the prediction uncertainty. These realizations can be considered as possible LF configurations.

Likelihood model

The likelihood model defines the likelihood of the LF classes given well observations and seismic data. We assume the well observations and seismic data to be collected independently, which entails conditional independence between well and seismic data expressed by

$$p(\mathbf{d}|\boldsymbol{\pi}) = p(\mathbf{d}^w|\boldsymbol{\pi})\, p(\mathbf{d}^s|\boldsymbol{\pi}) \tag{2}$$

where $p(\mathbf{d}^w|\boldsymbol{\pi})$ is a well likelihood model and $p(\mathbf{d}^s|\boldsymbol{\pi})$ a seismic likelihood model.

The well likelihood model is defined from locationwise observations of LF characteristics along the well profiles given by

$$[d^w_{\mathbf{x},t}|\pi_{\mathbf{x},t}] = \mu_{\pi_{\mathbf{x},t}} + e^w_{\mathbf{x},t} \tag{3}$$

where $\mu_{\pi_{\mathbf{x},t}}$ is the expected well observation response for LF class $\pi_{\mathbf{x},t}$, and $e^w_{\mathbf{x},t}$ is a spatially independent Gaussian error term. The relation defines the likelihood model

$$p(\mathbf{d}^w|\boldsymbol{\pi}) = \prod_{\mathbf{x}\in\mathcal{K}} \prod_t p(d^w_{\mathbf{x},t}|\pi_{\mathbf{x},t}) \tag{4}$$

where $\mathcal{K}$ are the well locations in $\mathcal{L}^{\mathbf{x}}_{\mathcal{D}}$ and the product in t is taken over $\mathcal{L}^t_{\mathcal{D}}$.

A decomposition like in Larsen et al. (2006) is used in the seismic likelihood model, and it is expressed

$$p(\mathbf{d}^s|\boldsymbol{\pi}) = \int \ldots \int p(\mathbf{d}^s|\mathbf{m})\, p(\mathbf{m}|\boldsymbol{\pi})\, d\mathbf{m} \tag{5}$$

where $p(\mathbf{d}^s|\mathbf{m})$ is a seismic likelihood model and $p(\mathbf{m}|\boldsymbol{\pi})$ a rock physics likelihood model. The integral is over the three elastic parameters in the target zone; hence computer demanding to determine.

The rock physics likelihood model can be factorized

$$p(\mathbf{m}|\boldsymbol{\pi}) = \prod_{\mathbf{x}} \prod_{t} p(\mathbf{m}_{\mathbf{x},t}|\pi_{\mathbf{x},t}) \tag{6}$$

with $\mathbf{x}$ taken over $\mathcal{L}_{\mathcal{D}}^{\mathbf{x}}$ and t taken over $\mathcal{L}_{\mathcal{D}}^{t}$ when not explicitly expressed. Hence the rock physics model is assumed to include variables in only one spatial location, see Avseth et al. (2005).

The relation between $\mathbf{d}^s$ and $\mathbf{m}$ is defined by the vertical convolution model like in Buland and Omre (2003)

$$[\mathbf{d}^s|\mathbf{m}] = \mathbf{WADm} + \mathbf{e} \tag{7}$$

where $\mathbf{A}$ is a matrix of angle-dependent weak contrast Aki-Richards coefficients, see Aki and Richards (1980), $\mathbf{D}$ is a differential matrix giving the contrasts of the elastic properties in $\mathbf{m}$, $\mathbf{W}$ is a block-diagonal convolution matrix containing one wavelet for each time-angle

8

gather, and $\mathbf{e}$ is Gaussian observation error. Using this relation, the seismic likelihood model is expressed like in Larsen et al. (2006)

$$p(\mathbf{d}^s|\mathbf{m}) = \text{const} \times \frac{p_*(\mathbf{m}|\mathbf{d}^s)}{p_*(\mathbf{m})} \tag{8}$$

where const is a general constant and $p_*(\mathbf{m}|\mathbf{d}^s)$ and $p_*(\mathbf{m})$ are Gaussian posterior and prior pdf's for linearized Zoeppritz AVO inversion, see Buland and Omre (2003). Note that the posterior pdf $p_*(\mathbf{m}|\mathbf{d}^s)$ can be calculated extremely fast in the Fourier domain, see Buland et al. (2003).

Prior model

The prior model contains our a priori knowledge about the 3D LF characteristics in the reservoir before any observations are made. Horizontally, we expect the LF characteristics to have extensive isotropic continuity. The LF characteristics are further expected to appear in certain sequences vertically, since lithologies are generated by sedimentary processes and fluids are segregated by gravity. Hence, the ordering of LF classes should be modeled nonsymmetrically, nonstationary in the vertical direction. In order to model this a priori information about the LF classes, we define the prior model to be a profile Markov random field.

The profile Markov random field is defined by

$$p(\boldsymbol{\pi}_\mathbf{x}|\boldsymbol{\pi}_{-\mathbf{x}}) = p(\boldsymbol{\pi}_\mathbf{x}|\boldsymbol{\pi}_\mathbf{y}; \mathbf{y} \in \delta(\mathbf{x})); \text{ all } \mathbf{x} \in \mathcal{L}_\mathcal{D}^\mathbf{x} \tag{9}$$

where $\boldsymbol{\pi}_\mathbf{x} : \{\pi_{\mathbf{x},t}; t \in \mathcal{L}_\mathcal{D}^t\}$ is a vertical LF profile in an arbitrary $\mathbf{x}$ in $\mathcal{L}_\mathcal{D}^\mathbf{x}$, $\boldsymbol{\pi}_{-\mathbf{x}} : \{\boldsymbol{\pi}_\mathbf{y}; \mathbf{y} \in \mathcal{L}_\mathcal{D}^\mathbf{x}, \mathbf{y} \neq \mathbf{x}\}$ is the set of all LF profiles except $\boldsymbol{\pi}_\mathbf{x}$, and $\delta(\mathbf{x})$ is a fixed neighborhood around $\mathbf{x}$

in $\mathcal{L}_{\mathcal{D}}^{\mathbf{x}}$. Hence, given all LF classes in the target zone except in profile $\boldsymbol{\pi}_{\mathbf{x}}$, the LF profile $\boldsymbol{\pi}_{\mathbf{x}}$ is dependent only upon the LF profiles in a predefined neighborhood $\delta(\mathbf{x})$ around $\mathbf{x}$. According to the Hammersley-Clifford theorem, the set of all conditional pmf's fully specify the Markov random field, see Besag (1974).

To model vertical orderings of the fluids, we let the LF profiles $\boldsymbol{\pi}_{\mathbf{x}}$ be defined by nonhomogeneous Markov chain models upwards through the target zone

$$p(\boldsymbol{\pi}_{\mathbf{x}}|\boldsymbol{\pi}_{\mathbf{y}}; \mathbf{y} \in \delta(\mathbf{x})) = \prod_{t} p(\pi_{\mathbf{x},t}|\pi_{\mathbf{x},t+1}, \pi_{\mathbf{y},t}; \mathbf{y} \in \delta(\mathbf{x})); \text{ all } \mathbf{x} \in \mathcal{L}_{\mathcal{D}}^{\mathbf{x}} \tag{10}$$

with $p(\pi_{\mathbf{x},T}|\pi_{\mathbf{x},T+1}, \pi_{\mathbf{y},T}; \mathbf{y} \in \delta(\mathbf{x})) = p(\pi_{\mathbf{x},T}|\pi_{\mathbf{y},T}; \mathbf{y} \in \delta(\mathbf{x}))$ for notational convenience. This Markov chain model corresponds to the model in Larsen et al. (2006) where it is demonstrated to be reliable in modeling petroleum reservoirs.

The upward transition probabilities for LF classes between two horizons in a profile, i.e., from $t+1$ to t, can be expressed as the transition matrix $\mathbf{P}^{t}(\pi_{\mathbf{y},t}; \mathbf{y} \in \delta(\mathbf{x}))$ where the elements are the conditional pmf's $p(\pi_{\mathbf{x},t}|\pi_{\mathbf{x},t+1}, \pi_{\mathbf{y},t}; \mathbf{y} \in \delta(\mathbf{x}))$ for all configurations of $(\pi_{\mathbf{x},t}, \pi_{\mathbf{x},t+1})$. The transition matrices are dependent on the time reference t through $\{\pi_{\mathbf{y},t}; \mathbf{y} \in \delta(\mathbf{x})\}$; hence the Markov chain is nonhomogeneous.

It can be demonstrated, see Appendix A, that the assumptions made for the profile Markov random field entail that

$$p(\pi_{\mathbf{x},t}|\boldsymbol{\pi}_{-(\mathbf{x},t)}) = p(\pi_{\mathbf{x},t}|\pi_{\mathbf{x},t-1}, \pi_{\mathbf{x},t+1}, \pi_{\mathbf{y},t}; \mathbf{y} \in \delta(\mathbf{x})); \text{ all } (\mathbf{x},t) \in \mathcal{L}_{\mathcal{D}} \tag{11}$$

with $\boldsymbol{\pi}_{-(\mathbf{x},t)} : \{\pi_{\mathbf{y},s}; (\mathbf{y},s) \in \mathcal{L}_{\mathcal{D}}, (\mathbf{y},s) \neq (\mathbf{x},t)\}$ hence $\boldsymbol{\pi}$ is a Markov random field in the tra-

ditional sense, see Besag (1974). This property can be used to ensure that the prior model is consistent in a probabilistic sense. There are, however, several advantages in defining the prior model as a profile Markov random field. Dependency structures in the lateral and vertical directions are clearly separated, which is suitable for reservoir modeling. Dependencies in the vertical direction can be formulated as a nonsymmetric, nonstationary Markov chain which is suitable for modeling both sedimentary processes and gravity segregation of fluids. Furthermore, a simulation algorithm which allows analytical treatment in the vertical direction and only requires an iterative procedure in the horizontal domain can be defined.

Posterior model

The posterior model is uniquely defined by the likelihood and prior models, and it is given by

$$
\begin{aligned}
p(\boldsymbol{\pi}|\mathbf{d}) = \text{const} \times &\prod_{\mathbf{x}\in\mathcal{K}}\prod_t p(d_{\mathbf{x},t}^w|\pi_{\mathbf{x},t}) \\
&\times \left[\int\ldots\int \frac{p_*(\mathbf{m}|\mathbf{d}^s)}{p_*(\mathbf{m})}\,\prod_{\mathbf{x}}\prod_t p(\mathbf{m}_{\mathbf{x},t}|\pi_{\mathbf{x},t})\,d\mathbf{m}\right]\,p(\boldsymbol{\pi}),
\end{aligned}
\tag{12}
$$

where const is a normalizing constant. The integral is over all configurations of the three elastic parameters in the target zone; hence very difficult to determine. An approximation along the lines of Larsen et al. (2006) is made in order to reduce the dimension of the integral. In the approximation, correlations within $\mathbf{m}$ and $\mathbf{m}|\mathbf{d}^s$ are ignored, and only the diagonal elements of the covariance matrices in the Gaussian pdf's $p_*(\mathbf{m})$ and $p_*(\mathbf{m}|\mathbf{d}^s)$ are used. This approximation has proved to be reliable in the 1D case, see Hammer and Ulvmoen (2008). The approximate posterior model is expressed

$$\tilde{p}(\boldsymbol{\pi}|\mathbf{d}) = \text{const} \times \prod_{\mathbf{x} \in \mathcal{K}} \prod_t p(d_{\mathbf{x},t}^w|\pi_{\mathbf{x},t}) \prod_{\mathbf{x}} \prod_t l(\mathbf{d}^s|\pi_{\mathbf{x},t}) \, p(\boldsymbol{\pi}), \tag{13}$$

where

$$l(\mathbf{d}^s|\pi_{\mathbf{x},t}) = \int \int \int \frac{p_*(\mathbf{m}_{\mathbf{x},t}|\mathbf{d}^s)}{p_*(\mathbf{m}_{\mathbf{x},t})} \, p(\mathbf{m}_{\mathbf{x},t}|\pi_{\mathbf{x},t}) \, d\mathbf{m}_{\mathbf{x},t} \tag{14}$$

is the approximated likelihood model. The integral is now of dimension three, and numerically tractable. The normalizing constant defined by $\sum_{\boldsymbol{\pi}} \tilde{p}(\boldsymbol{\pi}|\mathbf{d}) = 1$ is computer demanding as it is the sum over all combinations of LF classes in the target zone.

The prior model follows a Markov random field model; hence with a likelihood function that factorizes it is known, see Besag (1974), that the associated approximate conditional posterior model can be expressed

$$\tilde{p}(\boldsymbol{\pi}_{\mathbf{x}}|\boldsymbol{\pi}_{-\mathbf{x}},\mathbf{d}) = \begin{cases} \text{const} \times \prod_t l(\mathbf{d}^s|\pi_{\mathbf{x},t}) \, p(\pi_{\mathbf{x},t}|\pi_{\mathbf{x},t+1},\pi_{\mathbf{y},t}; \mathbf{y} \in \delta(\mathbf{x})); \text{ all } \mathbf{x} \in -\mathcal{K} \\[2ex] \text{const} \times \prod_t p(d_{\mathbf{x},t}^w|\pi_{\mathbf{x},t}) \, l(\mathbf{d}^s|\pi_{\mathbf{x},t}) \, p(\pi_{\mathbf{x},t}|\pi_{\mathbf{x},t+1},\pi_{\mathbf{y},t}; \mathbf{y} \in \delta(\mathbf{x})); \text{ all } \mathbf{x} \in \mathcal{K} \end{cases} \tag{15}$$

with the set $-\mathcal{K}$ containing all elements in $\mathcal{L}_{\mathcal{D}}^{\mathbf{x}}$ except the ones in $\mathcal{K}$, i.e., all horizon locations except the well locations. This block Markov formulation of the posterior model will be used to define an efficient simulation algorithm.

ASSESSMENT OF POSTERIOR MODEL

In Expression (15), conditional posterior pmf's are expressed for all $\mathbf{x} \in \mathcal{L}_{\mathcal{D}}^{\mathbf{x}}$. These conditional posterior models are on the same form as the 1D posterior model in Larsen et al.

(2006) except for the nonhomogeneneity in the prior model. The upward-downward recursive algorithm used to explore the posterior model in Larsen et al. (2006) is, however, also valid for nonhomogeneous Markov chain prior models, see Chib (1996). Hence, the conditional model in Expression (15) can be simulated exactly by the efficient upward-downward recursive algorithm. Laterally, a block Gibbs simulation algorithm may be used since the profile Markov random field is specified by a complete set of multivariate conditional pmf's. In the Gibbs simulation algorithm, direct computation of the normalizing constant is avoided.

The Gibbs sampler algorithm is fully described in Appendix B, and an outline of the algorithm is as follows:

Simulation Algorithm

Initiate

   Generate arbitrary $\boldsymbol{\pi}$

Iterate

   Draw $\mathbf{x}$ uniform randomly from $\mathcal{L}_{\mathcal{D}}^{\mathbf{x}}$

   Generate $\boldsymbol{\pi}_{\mathbf{x}}$ from $\tilde{p}(\boldsymbol{\pi}_{\mathbf{x}}|\boldsymbol{\pi}_{-\mathbf{x}},\mathbf{d})$ by the upward-downward simulation algorithm

The algorithm converges such that in the limit $\boldsymbol{\pi}$ will be a sample from $\tilde{p}(\boldsymbol{\pi}|\mathbf{d})$. Note that although the model is defined in 3D, the iterative Gibbs simulation algorithm only operates in 2D. The third dimension is simulated exactly by the very fast recursive upward-downward algorithm.

EMPIRICAL STUDY

In the empirical study on a realistic synthetic test case, we focus on two aspects. Firstly, we evaluate the general quality of the inversion approach. The LF characteristics are simulated and predicted both from seismic AVO data with low signal-to-noise ratio and from seismic AVO signal without observation error. Secondly, we evaluate the ability to identify thin laterally extensive layers of shale. This identification is made possible by improved resolution in the inversion. These thin layers of shale are particularly important since they have large impact on fluid flow.

We perform an empirical study on a reference 2D synthetic reservoir which we have made manually. The reference reservoir $\boldsymbol{\pi}$ contains the four LF classes gas-saturated sandstone, oil-saturated sandstone, brine-saturated sandstone, and shale, and it is presented in Figure 1. The target zone is defined from 2000 ms to 2284 ms vertically, discretized into units of one ms corresponding to the seismic sampling density; hence $T = 284$. Horizontally, 100 CMP profiles are considered. In the reservoir, many layers of shale are thin with considerable lateral extensions. These shale layers, in the range 1-3 ms thick, are much thinner than in Larsen et al. (2006), and far below what is normally referred to as seismic resolution.

The prior model is defined as a profile Markov random field, with the profiles defined as nonhomogeneous Markov chain models upwards through the reservoir as described in the previous section. We term this model a 2D Markov random field. The transitions up the profiles in $\mathbf{x} \in \mathcal{L}_{\mathcal{D}}^{\mathbf{x}}$ given the rest of the field are expressed as the transition matrices $\mathbf{P}^t(\pi_{\mathbf{y},t}; \mathbf{y} \in \delta(\mathbf{x}))$ where the elements are the conditional pmf's $p(\pi_{\mathbf{x},t}|\pi_{\mathbf{x},t+1}, \pi_{\mathbf{y},t}; \mathbf{y} \in \delta(\mathbf{x}))$ for all (4×4) configurations of $(\pi_{\mathbf{x},t}, \pi_{\mathbf{x},t+1})$. We consider a first order neighborhood in each lateral direction such that $\delta(\mathbf{x}) = (\mathbf{x} - 1, \mathbf{x} + 1)$ giving 16 possible neighborhoods, but by lateral symmetry

the number of neighborhoods is reduced to 10. The transition matrices are constructed such that most probability is assigned to transitions into LF classes identical to the neighboring ones, and low probability to other transitions. The transition matrix with the neighbors being oil-saturated sandstone and shale is for example

$$\mathbf{P}^t_{SO,SH} = \begin{pmatrix} 0.0005 & 0 & 0 & 0.9995 \\ 0.0002 & 0.4999 & 0 & 0.4999 \\ 0.0002 & 0.4998 & 0.0002 & 0.4998 \\ 0.0002 & 0.4998 & 0.0002 & 0.4998 \end{pmatrix}$$

with rows and columns corresponding to gas-, oil-, brine-saturated sandstone, and shale, respectively. Note that the transitions with zero probability in the matrix are the same as in Larsen et al. (2006), and they ensure ordering of the fluids according to gravity. We use the limiting distribution of the transition matrices as initial distributions. All the transition matrices and corresponding limiting distributions are fully described in Appendix C. In Larsen et al. (2006) the inversion model is defined profilewise, and the approximate posterior model is calculated exactly by the recursive upward-downward algorithm. In the current study, a more time consuming Gibbs sampling must be used. We also apply the profilewise Markov chain prior model defined in Larsen et al. (2006), and compare the results to the 2D Markov random field prior model of the current study. For the profilewise Markov chain prior model, the stationary transition matrix is calculated from the reference reservoir. The transition matrix and corresponding limiting distribution are specified in Appendix C. We also use a locationwise prior model without spatial coupling, see Larsen et al. (2006). In this prior model, the limiting distribution in the profilewise Markov chain model is used. This limiting distribution corresponds to the fraction of each LF class in the reference reservoir.

We use well observations in two well locations $\mathcal{K} : \{20, 80\}$. The well observations $\mathbf{d}^w$ are exact observations of LF classes along the profiles, presented in Figure 2. The well likelihood model is defined from exact locationwise observations of these LF characteristics.

The rock physics likelihood model $p(\mathbf{m}_{\mathbf{x},t}|\pi_{\mathbf{x},t})$ is a function in the three elastic parameters P-wave velocity, S-wave velocity, and density for each LF class. Like in Larsen et al. (2006), a set of representative samples from rock physics relations is defined to link the LF classes and the elastic parameters. The samples are presented in Figure 3. The elastic properties corresponding to the reference reservoir are obtained by using the mean value of $[\mathbf{m}_{\mathbf{x},t}|\pi_{\mathbf{x},t}]$ from the samples at each location and adding appropriate heterogeneity to make $\mathbf{m}$ appear realistic. The mean values for P-wave velocity, S-wave velocity, and density are $(3141, 1794, 2182)$, $(3199, 1758, 2274)$, $(3365, 1749, 2312)$ and $(3521, 1894, 2555)$ for gas-, oil-, brine-saturated sandstone, and shale, respectively.

The seismic likelihood model $p(\mathbf{d}^s|\mathbf{m})$ is defined by a convolutional model like in Buland and Omre (2003). The seismic signal is modeled profilewise for the five incidence angles $\boldsymbol{\theta} = (0°, 10°, 20°, 30°, 40°)$ and a Ricker wavelet with frequency 30 Hz and length 61 ms discretized over $\mathcal{L}_{\mathcal{D}}^t$ for all time-angle gathers. The observation error contains a mixture of zero mean vertical wavelet colored noise and white noise, see Buland and Omre (2003), and the variance in the colored noise is 100 times the variance in the white noise. The observation error is generated profilewise, then added to the seismic signal resulting in the seismic data. The signal-to-noise ratio in the seismic data is calculated as the ratio between the variance in the seismic signal and the variance in the observation error, and the value is 2.0. Figure 4 displays the synthetic prestack seismic data $\mathbf{d}^s$. The logarithm of the elastic material properties in $\mathbf{m}$ are approximated by a Gaussian random field parametrized by $(\boldsymbol{\mu}_*, \boldsymbol{\Sigma}_*, c_*(\tau))$ being

16

expectation vector, covariance matrix and spatial correlation function, respectively. The former two are calculated from the reference elastic parameters using standard statistical estimators, with values

$$\boldsymbol{\mu}_* = (8.117, 7.500, 7.770)$$

$$\boldsymbol{\Sigma}_* = \begin{pmatrix} 0.0075 & 0.0080 & 0.0035 \\ 0.0080 & 0.0114 & 0.0030 \\ 0.0035 & 0.0030 & 0.0043 \end{pmatrix}$$

corresponding to the logarithm of P-wave velocity, S-wave velocity, and density, respectively. We use a second order exponential spatial correlation function $c_*(\tau)$ with range of 3 ms. The integral in the likelihood model is obtained as the average of the functional value in 3000 samples specified for $[\mathbf{m}_{\mathbf{x},t}|\pi_{\mathbf{x},t}]$.

In the implementation of the algorithm, 30 ms of shale are added to the top and the bottom of the reservoir to avoid boundary effects. As lateral boundary conditions, we assume that the left- and right-most profiles have the same neighbor profiles on both sides, and the neighbor profiles are hence given double weights on the borders. We initiate the algorithm from four different configurations of $\boldsymbol{\pi}$ and monitor the proportion of the LF classes after each sweep, with one sweep corresponding to one update of each profile in the field. The sample paths are shown in Figure 5. All the initial configurations have converged to the same proportions after 2000 sweeps, which is defined to be the burn-in period. The simulation algorithm makes 120 sweeps every minute; hence burn-in is obtained after 16 minutes.

The expression $p_*(\mathbf{m}|\mathbf{d}^s)/p_*(\mathbf{m})$ is approximated by $\prod_{\mathbf{x}} p_*(\mathbf{m}_{\mathbf{x}}|\mathbf{d}_{\mathbf{x}}^s)/p_*(\mathbf{m}_{\mathbf{x}})$, and $p_*(\mathbf{m}_{\mathbf{x}})$ and

$p_*(\mathbf{m_x}|\mathbf{d_x})$ are computed like in Larsen et al. (2006) in the implementation. This implementational approximation will have only minor influence on the results in practice. The approach of Buland et al. (2003) could alternatively have been used on the full dimensions of $\mathbf{m}$ and $\mathbf{d}^s$.

RESULTS WITH DISCUSSION

Focus of the study is on the LF characteristics $\boldsymbol{\pi}$, and the complete solution is defined to be the approximate posterior model $\tilde{p}(\boldsymbol{\pi}|\mathbf{d})$ from which realizations can be generated and the most probable combination of LF characteristics can be determined. The marginal pmf's $\tilde{p}(\pi_{\mathbf{x},t}|\mathbf{d})$ are estimated by counting the number of occurrences of each of the LF classes at each location over 3600 realizations taken every 20 sweep after burn-in. We calculate the locationwise most probable solution from the expression

$$\hat{\pi}_{\mathbf{x},t} = \operatorname*{argmax}_{\pi_{\mathbf{x},t}} \tilde{p}(\pi_{\mathbf{x},t}|\mathbf{d}); \text{ all } (\mathbf{x},t) \in \mathcal{L}_{\mathcal{D}}. \tag{16}$$

Figure 6 contains three independent realizations of LF characteristics generated from the approximate posterior model $\tilde{p}(\boldsymbol{\pi}|\mathbf{d})$. Each realization can be considered as possible LF characteristics, and the set of realizations represents the prediction uncertainty in the solution. The structure in the realizations is the same, and all the realizations are realistic with respect to fluid segregation. The deviation between the realizations is small, indicating little prediction uncertainty.

Figure 7 and Table 1 contain a comparison between the predicted LF characteristics $\hat{\boldsymbol{\pi}}$ being the locationwise most probable solution and the reference LF characteristics $\boldsymbol{\pi}$, and a classifi-

cation matrix. In a perfect prediction $\hat{\boldsymbol{\pi}}$ would be identical to $\boldsymbol{\pi}$, and the classification matrix would contain zeroes in all entries except on the diagonal. The structure in the predicted solution and the reference case is mostly the same, but the reference LF characteristics are slightly more homogeneous than the locationwise most probable solution. The most probable solution is, on the other hand, more homogeneous than the realizations caused by uncertainty in the model. The well observations do not stand out, indicating that the inversion model is reliable in near-well areas, and that the information contained in the wells is an integral part of the inversion solution. The fluid segregation condition is fulfilled. All the diagonal elements in the classification matrix are the largest, and the proportions of the LF classes are largely correct. One of the main challenges of the study is to classify thin layers of shale, and we see from the prediction that layers down to one ms are identified. This is caused by the spatial coupling in the prior model which increases the probability of identification due to modeling of lateral continuity of shales. A few shale units are missed and a few artificial shale units are added, but the heterogeneity is largely correct.

Figure 8 contains a comparison between profiles $\mathbf{x} : \{21, 50, 79\}$ of the marginal approximate posterior model $\tilde{p}(\pi_{\mathbf{x},t}|\mathbf{d})$ with the reference LF classes marked on the respective axes. The former and latter profiles are the ones to the right and left, respectively, of the two wells, while profile $\mathbf{x} : \{50\}$ is the profile in the middle of the target zone. In a perfect classification, the probabilities would be one in the positions of the reference LF classes, and zero otherwise. It is difficult to distinguish the near- and off-well profiles by visual inspection. Both profile types imply high probability of classification to the true classes even for thin layers, and the probability of correct classification increases with increasing layer-thickness. All shale layers are found with high probability, even the ones that are very thin. The few misclassifications

19

occur with reduced probability.

Figure 9 and Table 2 contain a comparison between the predicted LF characteristics from three different prior models; first the 2D Markov random field prior model, second the profilewise Markov chain prior model, and last the locationwise prior model. In the profilewise Markov chain prediction the vertical orderings are correct with respect to fluid segregation. The well observations are not integrated in the solution, and we observe a skyline effect due to lack of horizontal continuity. The diagonal elements in the classification matrix are not always the largest, and the proportions of the LF classes deviate from the reference. The layers of shale are often too thick, and thin layers of sandstone between two layers of shale are filled with shale in many locations. The layers of shale are thinner and the prediction is much more homogeneous in the 2D Markov random field than in the profilewise Markov chain model. Much of the improvement in the 2D Markov random field model relative to the profilewise Markov chain model is in classification of gas-saturated sandstone, where spatial coupling in the prior model increase probability of identification. This is verified in the classification matrices. The locationwise prediction is very heterogeneous. It is, however, possible to recognize the structure from the reference reservoir, in particular the shale layers. Even though the locationwise prior model is independent in each location, the likelihood model is calculated given the full dimension of the seismic data including deconvolution. The prediction is therefore better than one could expect from a naive spatially independent model. The proportion of brine-saturated sandstone is overestimated while gas-saturated sandstone is severely underestimated. There is little horizontal continuity, and the fluid segregation condition is not fulfilled. The elements on the diagonal of the classification matrix are often small compared to the off-diagonal ones, and the proportions of the classes are not

correct. Thin layers of shale are often indicated in the prediction, but many artificial shale locations are added. The 2D Markov random field prediction is much more homogeneous than the locationwise prediction. Much of the gain in the 2D Markov random field model is in classification of gas- and oil-saturated sandstone, and in classification of thin shale layers.

Figure 10 contains a comparison between the marginal approximate posterior model $\tilde{p}(\pi_{\mathbf{x},t}|\mathbf{d})$ in profile $\mathbf{x} : \{50\}$ for the three prior models. The probabilities in the profilewise Markov chain model are smoothed between the layers making the transitions non-distinct. Most of the uncertainty appears in these interfaces. The probabilities in the 2D Markov random field model are more zero-one, and the probabilities are sharpened in the interfaces between the layers. The shale layers are thinner as result of these sharpenings. In the locationwise model, there is considerable fluctuation in the probabilities. Some probability of the correct LF class is often visible, indicating that the seismic data do contain some info regarding the LF classes. Most of the fluctuations are removed in the 2D Markov random field model compared to the locationwise model.

Figure 11 and Table 3 contain a comparison between the predicted and the reference LF characteristics from the inversion method based on the reference seismic signal without observation error. By visual inspection, the two are almost identical. The artificial layers of shale from the prediction with observation error are removed, and the layers of shale have almost correct thickness. The numbers on the diagonal of the classification matrix are much larger than the off-diagonal ones, and the proportions of the LF classes are almost correct. The results indicate that the inversion method is very reliable, and that the main problem is the noise in the observations.

Figure 12 contains a comparison between the predicted and the reference LF characteristics

from the inversion method without well observations. From the results it is clear that it is the seismic data, not the well observations, that give the structure in the solution. The well observations have impact only in the neighborhood of the well locations, and by defining some fluid contacts.

CONCLUSIONS

We have developed an efficient LF inversion approach from seismic data and well observations for 3D reservoirs. The inversion is defined in a Bayesian framework where the prior model for the LF classes is defined as a profile Markov random field with the vertical profiles following Markov chain models upward through the reservoir. The likelihood model is defined by a seismic forward model and rock-physics relations, and it is approximated in order to allow partial analytical treatment. The resulting posterior model is explored using an efficient block Gibbs simulation algorithm.

The inversion approach is evaluated empirically on a 2D synthetic reservoir. We compare the results from the fully coupled 2D Markov random field model with results from profilewise and locationwise models. The 2D model combines seismic data and well observations, and the latter is given lateral influence beyond the well locations. The fully coupled 2D model provides more trustworthy results than the profilewise and locationwise models, and it provides reliable classifications even with signal-to-noise ratio of two. LF units in the range 1-3 ms thick are identified due to lateral continuity, and this is far below what is normally considered to be the seismic resolution in profilewise interpretation. The approximation in the likelihood model appears very reliable as the inversion is almost correct in the no noise case. Hence the observation error is the major source of uncertainty.

The 3D simulation algorithm is very efficient as it is based on an analytical solution vertically, and McMC sampling only is needed in 2D laterally. Hence the algorithm is feasible to perform in 3D.

The LF inversion approach can be further extended by including vertical trends in the LF proportions. Simulation based estimation of model parameters is also possible due to the efficiency in the simulation algorithm.

The inversion approach is evaluated on a 2D cross section of a real reservoir in Ulvmoen et al. (2009).

APPENDIX A

MARKOV RANDOM FIELD

The profile Markov random field is defined by

$$p(\boldsymbol{\pi_x}|\boldsymbol{\pi_{-x}}) = p(\boldsymbol{\pi_x}|\boldsymbol{\pi_y}; \mathbf{y} \in \delta(\mathbf{x})); \text{ all } \mathbf{x} \in \mathcal{L}_{\mathcal{D}}^{\mathbf{x}} \tag{A-1}$$

where the profiles follow nonhomogeneous Markov chain models given by

$$p(\boldsymbol{\pi_x}|\boldsymbol{\pi_y}; \mathbf{y} \in \delta(\mathbf{x})) = \prod_t p(\pi_{\mathbf{x},t}|\pi_{\mathbf{x},t+1}, \pi_{\mathbf{y},t}; \mathbf{y} \in \delta(\mathbf{x})); \text{ all } \mathbf{x} \in \mathcal{L}_{\mathcal{D}}^{\mathbf{x}}. \tag{A-2}$$

Using this prior model formulation, we want to show

$$p(\pi_{\mathbf{x},t}|\boldsymbol{\pi_{-(\mathbf{x},t)}}) = p(\pi_{\mathbf{x},t}|\pi_{\mathbf{x},t+1}, \pi_{\mathbf{x},t-1}, \pi_{\mathbf{y},t}; \mathbf{y} \in \delta(\mathbf{x})); \text{ all } (\mathbf{x},t) \in \mathcal{L}_{\mathcal{D}}. \tag{A-3}$$

Proof:

$$
\begin{aligned}
p(\pi_{\mathbf{x},t}|\boldsymbol{\pi_{-(\mathbf{x},t)}}) &= p(\pi_{\mathbf{x},t}|\boldsymbol{\pi_{\mathbf{x},-t}}, \boldsymbol{\pi_y}; \mathbf{y} \in \delta(\mathbf{x})) \\[2mm]
&= \frac{p(\pi_{\mathbf{x},t}, \boldsymbol{\pi_{\mathbf{x},-t}}|\boldsymbol{\pi_y})}{\sum_{\pi_{\mathbf{x},t}} p(\pi_{\mathbf{x},t}, \boldsymbol{\pi_{\mathbf{x},-t}}|\boldsymbol{\pi_y})} \\[2mm]
&= \frac{p(\boldsymbol{\pi_x}|\boldsymbol{\pi_y})}{\sum_{\pi_{\mathbf{x},t}} p(\boldsymbol{\pi_x}|\boldsymbol{\pi_y})} \\[2mm]
&= \frac{p(\pi_{\mathbf{x},T}|\pi_{\mathbf{y},T}) \times \cdots \times p(\pi_{\mathbf{x},t}|\pi_{\mathbf{x},t+1}, \pi_{\mathbf{y},t}) \times \cdots \times p(\pi_{\mathbf{x},1}|\pi_{\mathbf{x},2}, \pi_{\mathbf{y},1})}{\sum_{\pi_{\mathbf{x},t}} p(\pi_{\mathbf{x},T}|\pi_{\mathbf{y},T}) \times \cdots \times p(\pi_{\mathbf{x},t}|\pi_{\mathbf{x},t+1}, \pi_{\mathbf{y},t}) \times \cdots \times p(\pi_{\mathbf{x},1}|\pi_{\mathbf{x},2}, \pi_{\mathbf{y},1})} \\[2mm]
&= \frac{p(\pi_{\mathbf{x},t+1}|\pi_{\mathbf{y},t+1})}{p(\pi_{\mathbf{x},t+1}|\pi_{\mathbf{y},t+1})} \times \frac{p(\pi_{\mathbf{x},t}|\pi_{\mathbf{x},t+1}, \pi_{\mathbf{y},t})\, p(\pi_{\mathbf{x},t-1}|\pi_{\mathbf{x},t}, \pi_{\mathbf{y},t-1})}{\sum_{\pi_{\mathbf{x},t}} p(\pi_{\mathbf{x},t}|\pi_{\mathbf{x},t+1}, \pi_{\mathbf{y},t})\, p(\pi_{\mathbf{x},t-1}|\pi_{\mathbf{x},t}, \pi_{\mathbf{y},t-1})} \\[2mm]
&= \frac{p(\pi_{\mathbf{x},t+1}, \pi_{\mathbf{x},t}, \pi_{\mathbf{x},t-1}|\pi_{\mathbf{y},t+1}, \pi_{\mathbf{y},t}, \pi_{\mathbf{y},t-1})}{\sum_{\pi_{\mathbf{x},t}} p(\pi_{\mathbf{x},t+1}, \pi_{\mathbf{x},t}, \pi_{\mathbf{x},t-1}|\pi_{\mathbf{y},t+1}, \pi_{\mathbf{y},t}, \pi_{\mathbf{y},t-1})} \\[2mm]
&= p(\pi_{\mathbf{x},t}|\pi_{\mathbf{x},t+1}, \pi_{\mathbf{x},t-1}, \pi_{\mathbf{y},t+1}, \pi_{\mathbf{y},t}, \pi_{\mathbf{y},t-1}) \\[2mm]
&= p(\pi_{\mathbf{x},t}|\pi_{\mathbf{x},t+1}, \pi_{\mathbf{x},t-1}, \pi_{\mathbf{y},t}; \mathbf{y} \in \delta(\mathbf{x})).
\end{aligned}
$$

$$\tag{A-4}$$

APPENDIX B

SIMULATION ALGORITHM

Initiate

   Generate arbitrary $\boldsymbol{\pi}^1$

Iterate

   $i = 2, 3, \ldots$

   Initiate

    $\boldsymbol{\pi}^i = \boldsymbol{\pi}^{i-1}$

   Iterate

   Draw $\mathbf{x}$ uniform randomly from $\mathcal{L}_{\mathcal{D}}^{\mathbf{x}}$

Upward Recursion

   Initiate

$$p_u(\pi_{\mathbf{x},T}^c) = \begin{cases} \text{const} \times l(\mathbf{d}^s|\pi_{\mathbf{x},T}^c)\, p(\pi_{\mathbf{x},T}^c|\pi_{\mathbf{y},T}^i); \ \mathbf{x} \in -\mathcal{K} \\[1.5em] \text{const} \times p(d_{\mathbf{x},T}^w|\pi_{\mathbf{x},T}^c)\, l(\mathbf{d}^s|\pi_{\mathbf{x},T}^c)\, p(\pi_{\mathbf{x},T}^c|\pi_{\mathbf{y},T}^i); \ \mathbf{x} \in \mathcal{K} \end{cases}$$

$$\text{const} = \left[\sum_{\pi_{\mathbf{x},T}} p_u(\pi_{\mathbf{x},T}^c) \right]^{-1}$$

   Iterate $t = T-1, T-2, \ldots, 1$

$$p_u(\pi_{\mathbf{x},t+1}^c, \pi_{\mathbf{x},t}^c) = \begin{cases} \text{const} \times l(\mathbf{d}^s|\pi_{\mathbf{x},t}^c)\, p(\pi_{\mathbf{x},t}^c|\pi_{\mathbf{x},t+1}^c, \pi_{\mathbf{y},t}^i)\, p_u(\pi_{\mathbf{x},t+1}^c); \ \mathbf{x} \in -\mathcal{K} \\[1.5em] \text{const} \times p(d_{\mathbf{x},t}^w|\pi_{\mathbf{x},t}^c)\, l(\mathbf{d}^s|\pi_{\mathbf{x},t}^c)\, p(\pi_{\mathbf{x},t}^c|\pi_{\mathbf{x},t+1}^c, \pi_{\mathbf{y},t}^i)\, p_u(\pi_{\mathbf{x},t+1}^c); \ \mathbf{x} \in \mathcal{K} \end{cases}$$

$$\text{const} = \left[\sum_{\pi_{\mathbf{x},t+1}} \sum_{\pi_{\mathbf{x},t}} p_u(\pi_{\mathbf{x},t+1}^c, \pi_{\mathbf{x},t}^c) \right]^{-1}$$

$$p_u(\pi_{\mathbf{x},t}^c) = \sum_{\pi_{\mathbf{x},t+1}} p_u(\pi_{\mathbf{x},t+1}^c, \pi_{\mathbf{x},t}^c)$$

   End iterate t

Downward Simulation

Initiate

Generate $\pi_{\mathbf{x},1}^c$ from $p_u(\pi_{\mathbf{x},1}^c)$

Iterate $t = 2 \dots, T$

Generate $\pi_{\mathbf{x},t}^c$ from $p_u(\pi_{\mathbf{x},t}^c | \pi_{\mathbf{x},t-1}^c) = p_u(\pi_{\mathbf{x},t}^c, \pi_{\mathbf{x},t-1}^c)/p_u(\pi_{\mathbf{x},t-1}^c)$

End iterate t

Update

$\pi_{\mathbf{x}}^i = \pi_{\mathbf{x}}^c$

End iterate $\mathbf{x}$

End iterate i

In each iteration i, $\boldsymbol{\pi}^i$ is generated from $\tilde{p}^i(\boldsymbol{\pi}|\mathbf{d})$ with limiting distribution

$$\lim_{i \to \infty} \tilde{p}^i(\boldsymbol{\pi}|\mathbf{d}) = \tilde{p}(\boldsymbol{\pi}|\mathbf{d}) \tag{B-1}$$

which is the distribution of interest.

APPENDIX C

TRANSITION MATRICES

Transition matrices in 2D Markov random field model

$$\mathbf{P}_{SG,SG}^t = \begin{pmatrix} 0.9998 & 0 & 0 & 0.0002 \\ 0.9996 & 0.0002 & 0 & 0.0002 \\ 0.9994 & 0.0002 & 0.0002 & 0.0002 \\ 0.9994 & 0.0002 & 0.0002 & 0.0002 \end{pmatrix} \quad \mathbf{P}_{SG,SO}^t = \begin{pmatrix} 0.9995 & 0 & 0 & 0.0005 \\ 0.4999 & 0.4999 & 0 & 0.0002 \\ 0.4998 & 0.4998 & 0.0002 & 0.0002 \\ 0.4998 & 0.4998 & 0.0002 & 0.0002 \end{pmatrix}$$

$$\mathbf{P}_{SG,SB}^t = \begin{pmatrix} 0.9995 & 0 & 0 & 0.0005 \\ 0.9990 & 0.0005 & 0 & 0.0005 \\ 0.4998 & 0.0002 & 0.4998 & 0.0002 \\ 0.4998 & 0.0002 & 0.4998 & 0.0002 \end{pmatrix} \quad \mathbf{P}_{SG,SH}^t = \begin{pmatrix} 0.5000 & 0 & 0 & 0.5000 \\ 0.4999 & 0.0002 & 0 & 0.4999 \\ 0.4998 & 0.0002 & 0.0002 & 0.4998 \\ 0.4998 & 0.0002 & 0.0002 & 0.4998 \end{pmatrix}$$

$$\mathbf{P}_{SO,SO}^t = \begin{pmatrix} 0.5000 & 0 & 0 & 0.5000 \\ 0.0002 & 0.9996 & 0 & 0.0002 \\ 0.0002 & 0.9994 & 0.0002 & 0.0002 \\ 0.0002 & 0.9994 & 0.0002 & 0.0002 \end{pmatrix} \quad \mathbf{P}_{SO,SB}^t = \begin{pmatrix} 0.5000 & 0 & 0 & 0.5000 \\ 0.0005 & 0.9990 & 0 & 0.0005 \\ 0.0002 & 0.4998 & 0.4998 & 0.0002 \\ 0.0002 & 0.4998 & 0.4998 & 0.0002 \end{pmatrix}$$

$$\mathbf{P}_{SO,SH}^t = \begin{pmatrix} 0.0005 & 0 & 0 & 0.9995 \\ 0.0002 & 0.4999 & 0 & 0.4999 \\ 0.0002 & 0.4998 & 0.0002 & 0.4998 \\ 0.0002 & 0.4998 & 0.0002 & 0.4998 \end{pmatrix} \quad \mathbf{P}_{SB,SB}^t = \begin{pmatrix} 0.5000 & 0 & 0 & 0.5000 \\ 0.3333 & 0.3333 & 0 & 0.3333 \\ 0.0002 & 0.0002 & 0.9994 & 0.0002 \\ 0.0002 & 0.0002 & 0.9994 & 0.0002 \end{pmatrix}$$

$$\mathbf{P}^t_{SB,SH} = \begin{pmatrix} 0.0005 & 0 & 0 & 0.9995 \\ 0.0005 & 0.0005 & 0 & 0.9990 \\ 0.0002 & 0.0002 & 0.4998 & 0.4998 \\ 0.0002 & 0.0002 & 0.4998 & 0.4998 \end{pmatrix} \mathbf{P}^t_{SH,SH} = \begin{pmatrix} 0.0002 & 0 & 0 & 0.9998 \\ 0.0002 & 0.0002 & 0 & 0.9996 \\ 0.0002 & 0.0002 & 0.0002 & 0.9994 \\ 0.0002 & 0.0002 & 0.0002 & 0.9994 \end{pmatrix}$$

with limiting distributions

$$\mathbf{P}^l_{SG,SG} = \begin{pmatrix} 0.9997 & 0.0000 & 0.0000 & 0.0003 \end{pmatrix} \mathbf{P}^l_{SG,SO} = \begin{pmatrix} 0.9990 & 0.0005 & 0.0000 & 0.0005 \end{pmatrix}$$

$$\mathbf{P}^l_{SG,SB} = \begin{pmatrix} 0.9990 & 0.0000 & 0.0005 & 0.0005 \end{pmatrix} \mathbf{P}^l_{SG,SH} = \begin{pmatrix} 0.4999 & 0.0001 & 0.0001 & 0.4999 \end{pmatrix}$$

$$\mathbf{P}^l_{SO,SO} = \begin{pmatrix} 0.0005 & 0.9990 & 0.0000 & 0.0005 \end{pmatrix} \mathbf{P}^l_{SO,SB} = \begin{pmatrix} 0.0010 & 0.9970 & 0.0010 & 0.0010 \end{pmatrix}$$

$$\mathbf{P}^l_{SO,SH} = \begin{pmatrix} 0.0002 & 0.4997 & 0.0001 & 0.4999 \end{pmatrix} \mathbf{P}^l_{SB,SB} = \begin{pmatrix} 0.0007 & 0.0004 & 0.9981 & 0.0007 \end{pmatrix}$$

$$\mathbf{P}^l_{SB,SH} = \begin{pmatrix} 0.0002 & 0.0002 & 0.4995 & 0.5000 \end{pmatrix} \mathbf{P}^l_{SH,SH} = \begin{pmatrix} 0.0002 & 0.0002 & 0.0002 & 0.9993 \end{pmatrix}$$

with the term $\mathbf{P}^t_{(\cdot,\cdot)}$ corresponding to the transition matrix with lateral neighbors $(\cdot, \cdot)$ and SG, SO, SB and SH corresponding to gas-, oil-, brine-saturated sandstone, and shale, respectively.

Transition matrix in profilewise Markov chain model

$$\mathbf{P} = \begin{pmatrix} 0.9001 & 0 & 0 & 0.0999 \\ 0.0531 & 0.8913 & 0 & 0.0557 \\ 0.0030 & 0.0560 & 0.9065 & 0.0345 \\ 0.0129 & 0.0097 & 0.0787 & 0.8987 \end{pmatrix}$$

with limiting distribution

$$\mathbf{P}^l = \begin{pmatrix} 0.1544 & 0.1870 & 0.3010 & 0.3576 \end{pmatrix}.$$

REFERENCES

Aki, K. and P. G. Richards, 1980, Quantitative seismology: Theory and methods: W. H. Freeman and Company.

Avseth, P., T. Mukerji, and G. Mavko, 2005, Quantitative seismic interpretation: Applying rock physics tools to reduce interpretation risk: Cambridge University Press.

Besag, J., 1974, Spatial interaction and the statistical analysis of lattice systems: Journal of the royal statistical society. Series B (Methodological), **36**, 192–236.

Buland, A., O. Kolbjørnsen, R. Hauge, Ø. Skjæveland, and K. Duffaut, 2008, Bayesian lithology and fluid prediction from seismic prestack data: Geophysics, **73**, no. 3, C13–C21.

Buland, A., O. Kolbjørnsen, and H. Omre, 2003, Rapid spatially coupled AVO inversion in the Fourier domain: Geophysics, **68**, 824–836.

Buland, A. and H. Omre, 2003, Bayesian linearized AVO inversion: Geophysics, **68**, 185–198.

Chib, S., 1996, Calculating posterior distributions and modal estimates in Markov mixture models: Journal of Econometrics, **75**, 79–97.

Eidsvik, J., P. Avseth, H. Omre, T. Mukerji, and G. Mavko, 2004, Stochastic reservoir characterization using prestack seismic data: Geophysics, **69**, 978–993.

González, E. F., T. Mukerji, and G. Mavko, 2008, Seismic inversion combining rock physics and multiple-point geostatistics: Geophysics, **73**, no. 1, R11–R21.

Hammer, H. and M. Ulvmoen, 2008, Empirical comparison of two Bayesian lithology-fluid prediction algorithms: Technical Report S5-2008, Department of Mathematical Sciences, Norwegian University of Science and Technology, Trondheim, Norway.

Larsen, A. L., M. Ulvmoen, H. Omre, and A. Buland, 2006, Bayesian lithology/fluid prediction and simulation on the basis of a Markov-chain prior model: Geophysics, **71**, no. 5, R69–R78.

Ulvmoen, M., H. Omre, and A. Buland, 2009, Improved resolution in Bayesian lithology/fluid inversion from prestack seismic data and well observations: Part II - Real case study: Geophysics, XXX.

field model (upper left); profilewise Markov chain model (upper right); and locationwise model (lower) with gas-saturated sandstone (red), oil-saturated sandstone (green), brine-saturated sandstone (blue), and shale (black).

10   Marginal approximate posterior $\tilde{p}(\pi_{\mathbf{x},t}|\mathbf{d})$ in profile $\mathbf{x} : \{50\}$ for 2D Markov random field model (upper left); profilewise Markov chain model (upper right); and locationwise model (lower) with gas-saturated sandstone, oil-saturated sandstone, brine-saturated sandstone, and shale denoted SG, SO, SB, and SH, respectively. Reference LF profile $\boldsymbol{\pi_x}$ is marked on respective axis.

11   Results from case without observation error, i.e., inversion based on reference seismic signal $\mathbf{s}$. Locationwise most probable LF characteristics prediction $\hat{\boldsymbol{\pi}}$ for 2D Markov random field model (left); and reference LF characteristics $\boldsymbol{\pi}$ (right) with gas-saturated sandstone (red), oil-saturated sandstone (green), brine-saturated sandstone (blue), and shale (black).

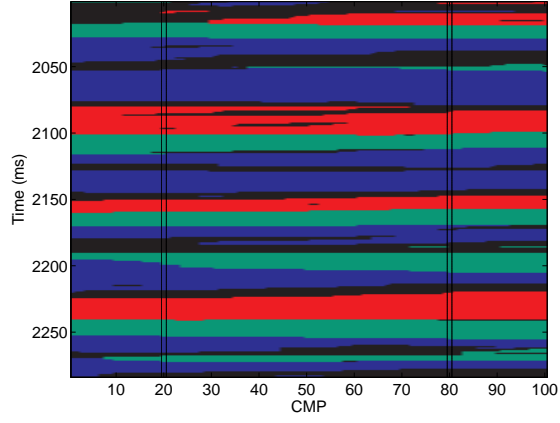12   Locationwise most probable LF characteristics prediction $\hat{\boldsymbol{\pi}}$ for 2D Markov random field model from inversion without well observations (left); and reference LF characteristics $\boldsymbol{\pi}$ (right) with gas-saturated sandstone (red), oil-saturated sandstone (green), brine-saturated sandstone (blue), and shale (black).

Figure 1: Reference LF characteristics $\boldsymbol{\pi}$ with gas-saturated sandstone (red), oil-saturated sandstone (green), brine-saturated sandstone (blue), and shale (black).
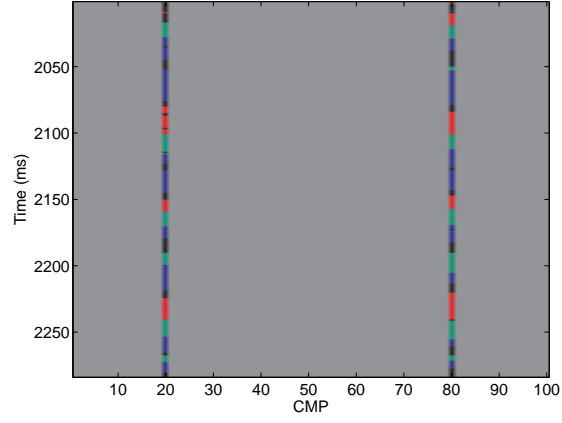
Figure 2: Well observations $\mathbf{d}^w$ in $\mathcal{K}$: $\{20, 80\}$ with gas-saturated sandstone (red), oil-saturated sandstone (green), brine-saturated sandstone (blue), and shale (black).
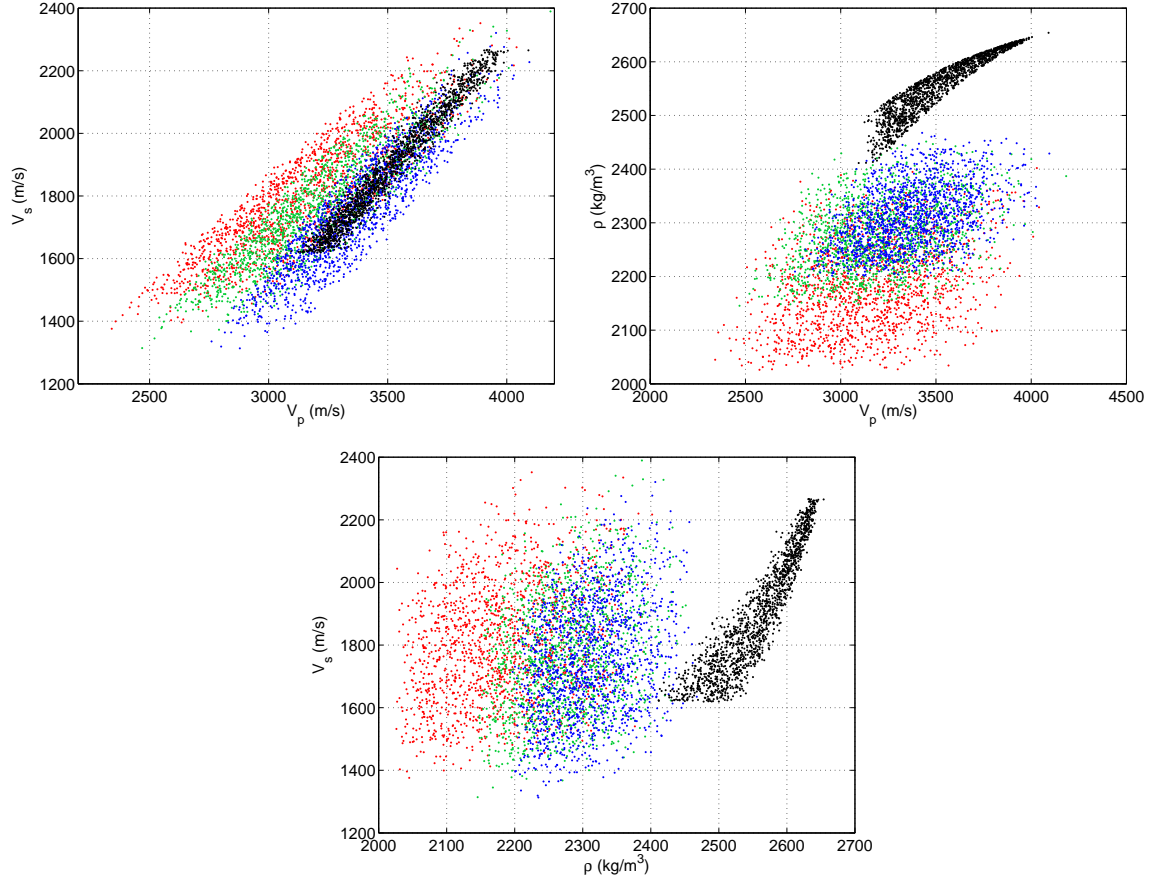
Figure 3: Elastic properties **m** represented by P-wave velocity (V_p), S-wave velocity (V_s), and density (ρ) given gas-saturated sandstone (red), oil-saturated sandstone (green), brine-saturated sandstone (blue), and shale (black) simulated from a rock physics model.
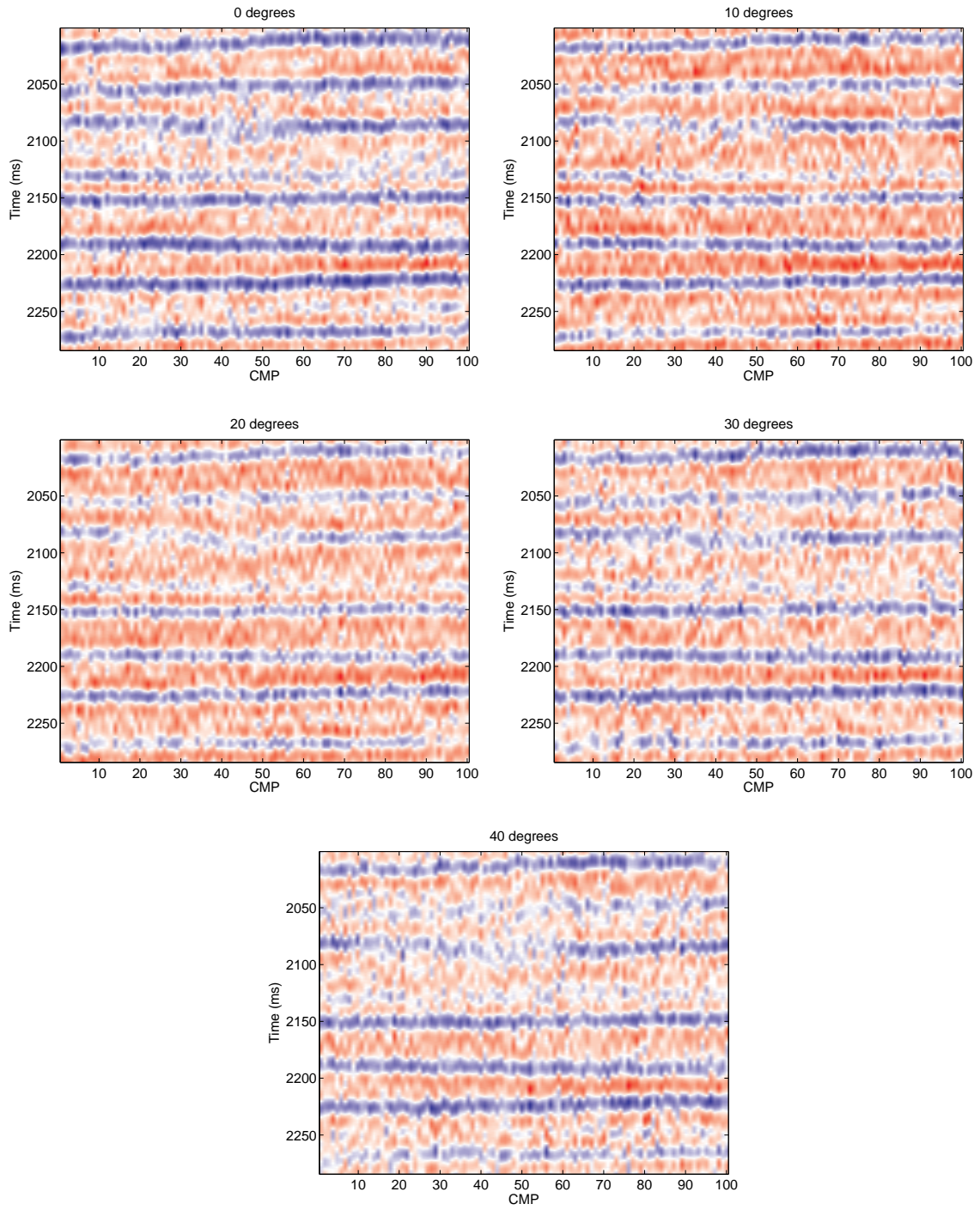
Figure 4: Synthetic prestack seismic data $\mathbf{d}^s$ for angles $\boldsymbol{\theta} = (0°, 10°, 20°, 30°, 40°)$, respectively.
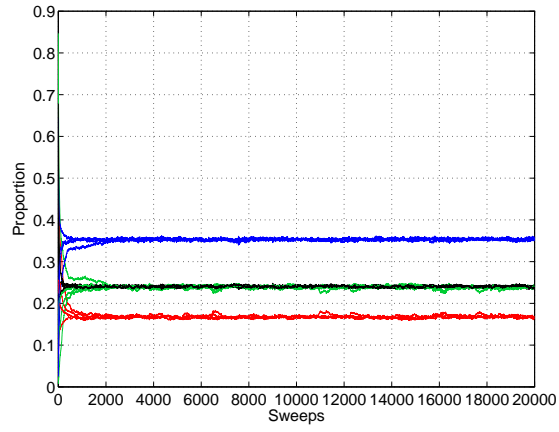
Figure 5: Convergence plot monitoring proportion of LF classes after each sweep of simulation algorithm with gas-saturated sandstone (red), oil-saturated sandstone (green), brine-saturated sandstone (blue), and shale (black).
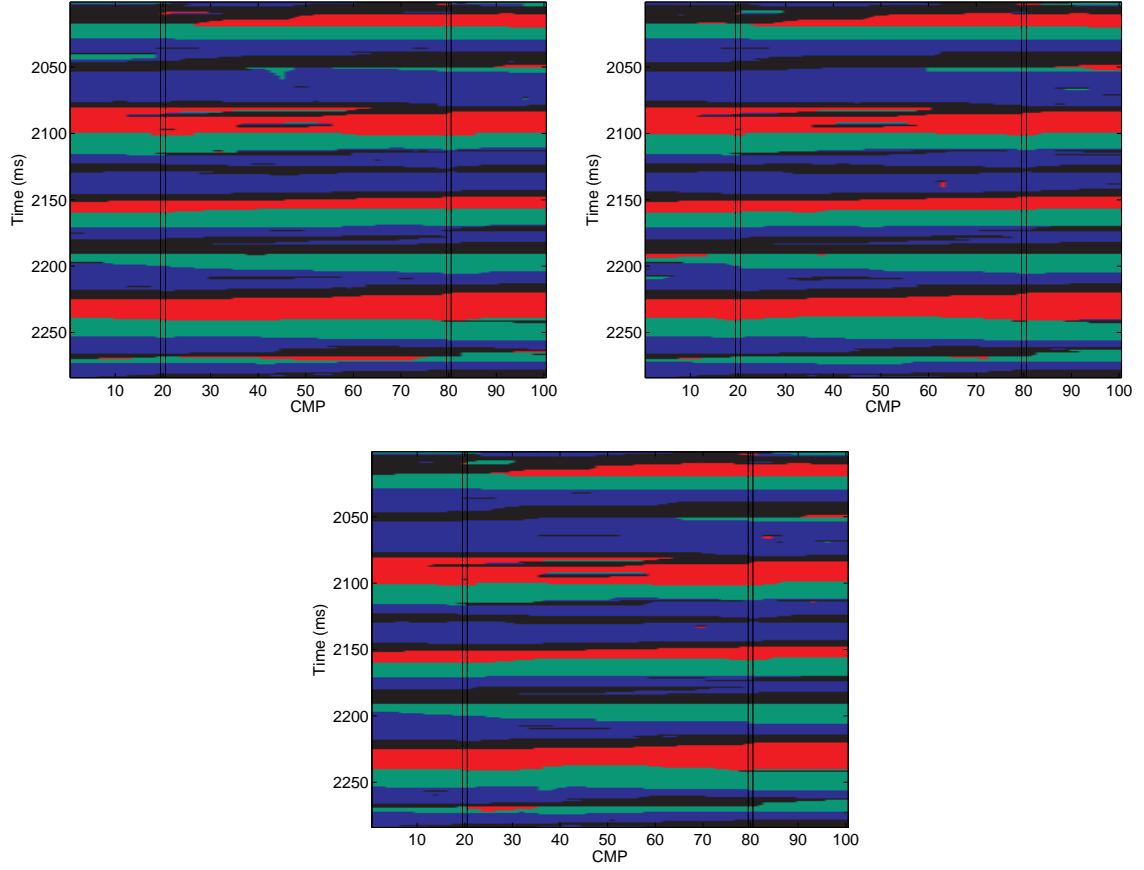
Figure 6: Independent realizations of LF characteristics from approximate posterior $\tilde{p}(\boldsymbol{\pi}|\mathbf{d})$ for 2D Markov random field model with gas-saturated sandstone (red), oil-saturated sandstone (green), brine-saturated sandstone (blue), and shale (black).
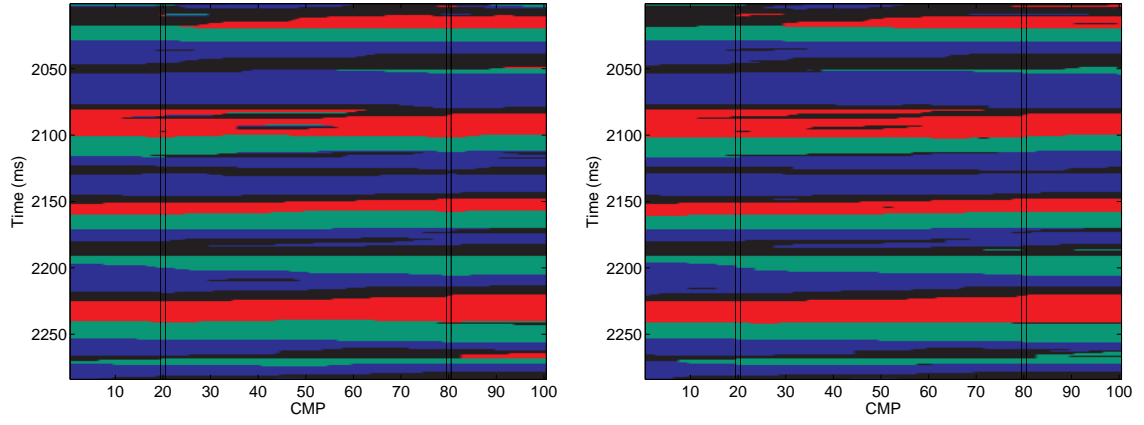
Figure 7: Locationwise most probable LF characteristics prediction $\hat{\boldsymbol{\pi}}$ for 2D Markov random field model (left); and reference LF characteristics $\boldsymbol{\pi}$ (right) with gas-saturated sandstone (red), oil-saturated sandstone (green), brine-saturated sandstone (blue), and shale (black).
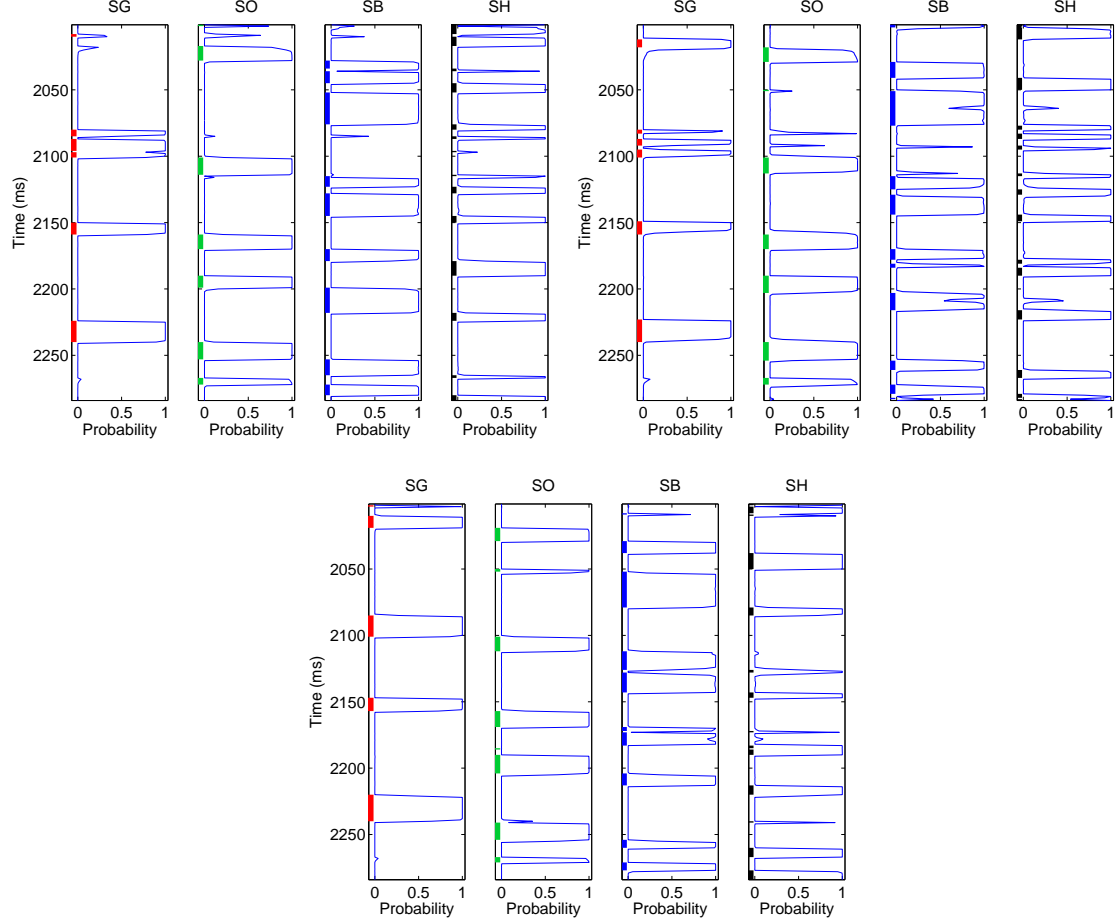
Figure 8: Marginal approximate posterior $\tilde{p}(\pi_{\mathbf{x},t}|\mathbf{d})$ for 2D Markov random field model in profiles $\mathbf{x} : \{21, 50, 79\}$ upper left, upper right and lower, respectively, with gas-saturated sandstone, oil-saturated sandstone, brine-saturated sandstone, and shale denoted SG, SO, SB, and SH, respectively. Reference LF profile $\boldsymbol{\pi_{\mathbf{x}}}$ is marked on respective axis.
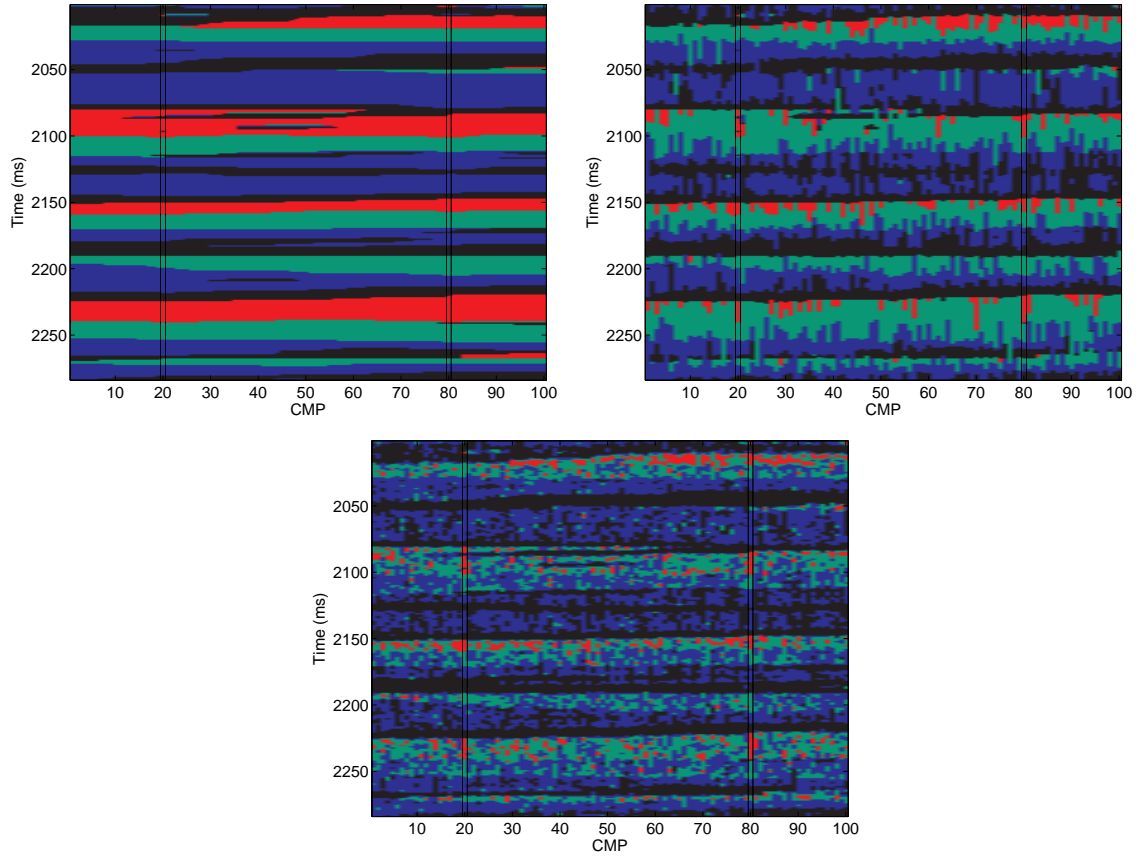
Figure 9: Locationwise most probable LF characteristics predictions $\hat{\boldsymbol{\pi}}$ for 2D Markov random field model (upper left); profilewise Markov chain model (upper right); and locationwise model (lower) with gas-saturated sandstone (red), oil-saturated sandstone (green), brine-saturated sandstone (blue), and shale (black).
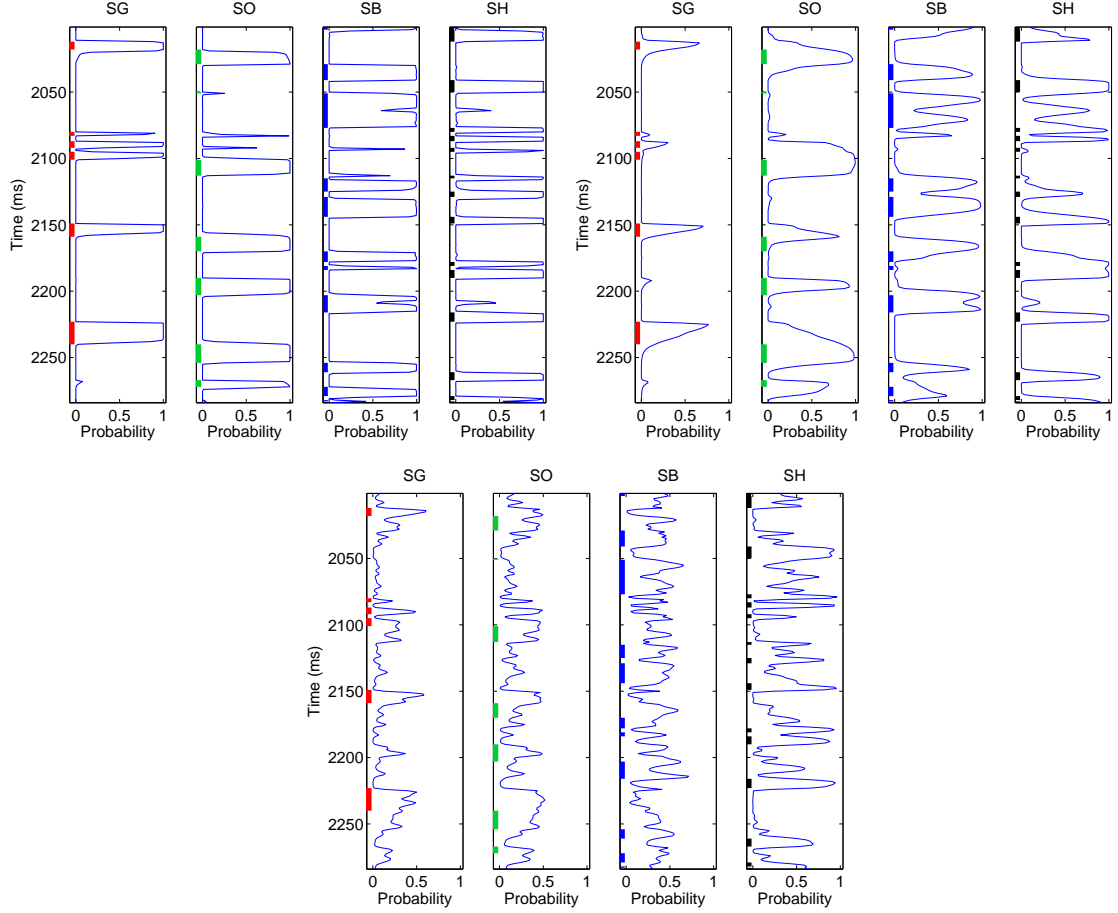
Figure 10: Marginal approximate posterior $\tilde{p}(\pi_{\mathbf{x},t}|\mathbf{d})$ in profile $\mathbf{x} : \{50\}$ for 2D Markov random field model (upper left); profilewise Markov chain model (upper right); and locationwise model (lower) with gas-saturated sandstone, oil-saturated sandstone, brine-saturated sandstone, and shale denoted SG, SO, SB, and SH, respectively. Reference LF profile $\boldsymbol{\pi}_{\mathbf{x}}$ is marked on respective axis.

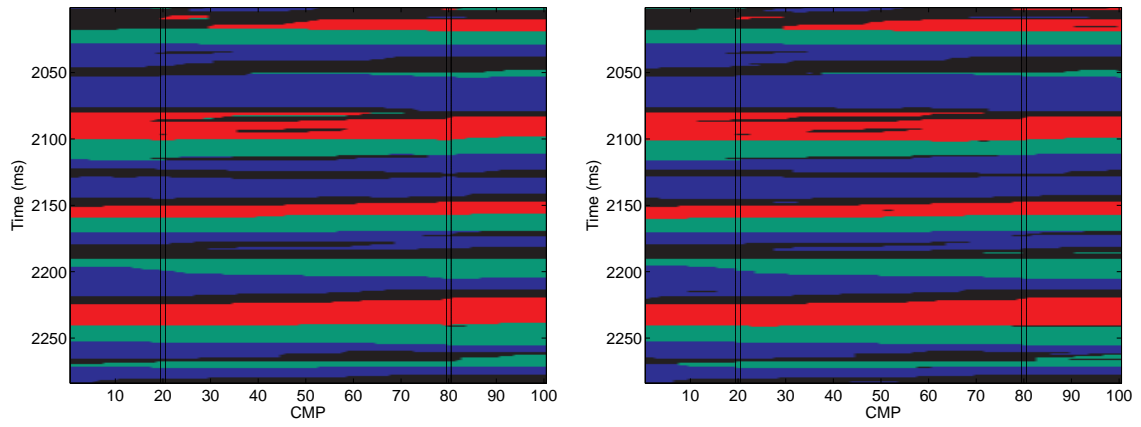Figure 11: Results from case without observation error, i.e., inversion based on reference seismic signal **s**. Locationwise most probable LF characteristics prediction $\hat{\boldsymbol{\pi}}$ for 2D Markov random field model (left); and reference LF characteristics $\boldsymbol{\pi}$ (right) with gas-saturated sandstone (red), oil-saturated sandstone (green), brine-saturated sandstone (blue), and shale (black).

Figure 12: Locationwise most probable LF characteristics prediction $\hat{\boldsymbol{\pi}}$ for 2D Markov random field model from inversion without well observations (left); and reference LF characteristics $\boldsymbol{\pi}$ (right) with gas-saturated sandstone (red), oil-saturated sandstone (green), brine-saturated sandstone (blue), and shale (black).
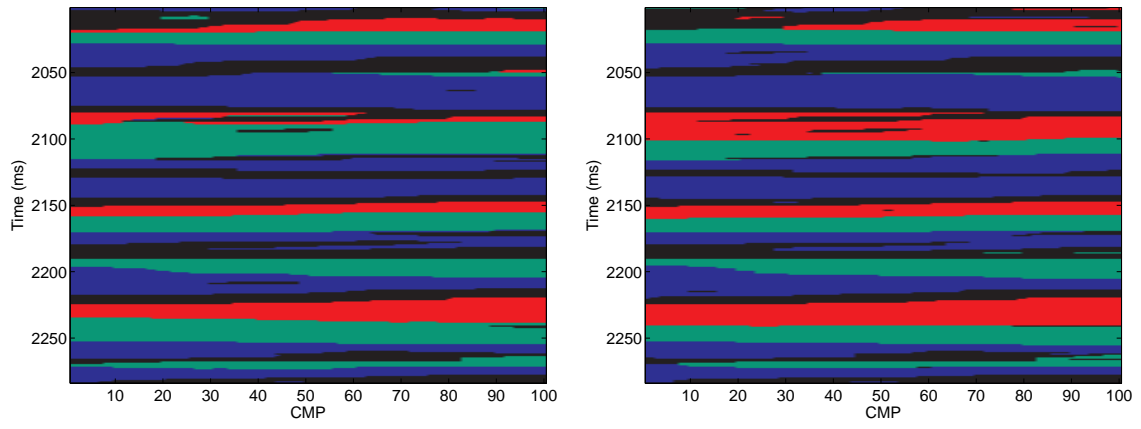
$\pi \diagdown \hat{\pi}$	SG	SO	SB	SH	Σ
SG	4605	365	42	13	5025
SO	94	6265	126	36	6521
SB	0	83	9798	639	10520
SH	51	44	169	6070	6334
Σ	4750	6757	10135	6758	

Table 1: Classification matrix for 2D Markov random field model with gas-saturated sandstone, oil-saturated sandstone, brine-saturated sandstone, and shale denoted SG, SO, SB, and SH, respectively.

$\pi \setminus \hat{\pi}$	SG	SO	SB	SH	Σ
SG	4605	365	42	13	5025
SO	94	6265	126	36	6521
SB	0	83	9798	639	10520
SH	51	44	169	6070	6334
Σ	4750	6757	10135	6758	

$\pi \setminus \hat{\pi}$	SG	SO	SB	SH	Σ
SG	1069	3759	115	82	5025
SO	111	4382	1904	124	6521
SB	0	575	7500	2445	10520
SH	34	193	767	5340	6334
Σ	1214	8909	10286	7991	

$\pi \setminus \hat{\pi}$	SG	SO	SB	SH	Σ
SG	921	2815	1258	31	5025
SO	217	2506	3594	204	6521
SB	3	300	6822	3395	10520
SH	0	44	609	5681	6334
Σ	1141	5665	12283	9311	

Table 2: Classification matrix for 2D Markov random field model; profilewise Markov chain model; and locationwise model with gas-saturated sandstone, oil-saturated sandstone, brine-saturated sandstone, and shale denoted SG, SO, SB, and SH, respectively.

$\boldsymbol{\pi} \diagdown \hat{\boldsymbol{\pi}}$	SG	SO	SB	SH	Σ
SG	4702	318	0	5	5025
SO	0	6418	84	19	6521
SB	0	59	9950	511	10520
SH	46	59	37	6192	6334
Σ	4748	6854	10071	6727	

Table 3: Classification matrix for inversion based on reference seismic signal **s** without observation error for 2D Markov random field model with gas-saturated sandstone, oil-saturated sandstone, brine-saturated sandstone, and shale denoted SG, SO, SB, and SH, respectively.